AGU PUBLICATIONS

JGR

Journal of Geophysical Research: Atmospheres

RESEARCH ARTICLE
10.1002/2015JD023318

Key Points:
- Waves dehydrate whereas convection and microphysics hydrate the 100 hPa level
- Waves and convection increase cloud occurrence frequency in the TTL
- Heating rate variability dehydrates and decreases TTL clouds

Correspondence to:
R. Ueyama,
rei.ueyama@nasa.gov

Citation:
Ueyama, R., E. J. Jensen, L. Pfister, and J.-E. Kim (2015), Dynamical, convective, and microphysical control on wintertime distributions of water vapor and clouds in the tropical tropopause layer, *J. Geophys. Res. Atmos.*, *120*, 10,483–10,500, doi:10.1002/2015JD023318.

Received 27 FEB 2015
Accepted 16 AUG 2015
Accepted article online 20 AUG 2015
Published online 3 OCT 2015

Dynamical, convective, and microphysical control on wintertime distributions of water vapor and clouds in the tropical tropopause layer

Rei Ueyama[1,2], Eric J. Jensen[1], Leonhard Pfister[1], and Ji-Eun Kim[3]

[1]NASA Ames Research Center, Moffett Field, California, USA, [2]Bay Area Environmental Research Institute, Petaluma, California, USA, [3]NorthWest Research Associates, CoRA Office, Boulder, Colorado, USA

Abstract Processes that influence the humidity and cirrus cloud abundance in the Tropical Tropopause Layer (TTL) during boreal winter 2006–2007 are investigated in simulations of clouds along backward trajectories of parcels ending at the 372 K potential temperature (100 hPa) level in the tropics. Trajectories are calculated using offline calculations of seasonal mean tropical radiative heating rates along with reanalysis temperature and wind data with enhanced wave-driven variability in the TTL. The one-dimensional (vertical) time-dependent cloud microphysical model is initialized with water vapor measurements from the Microwave Limb Sounder and the evolution of clouds along each trajectory is simulated using temperature profiles extracted from reanalysis data and convective cloud top heights estimated from 3-hourly geostationary satellite imagery. Averaged over the tropics, waves dehydrate the 100 hPa level by 0.5 ppmv, while convection and cloud microphysical processes moisten by 0.3 and 0.7 ppmv, respectively. The tropical mean cloud occurrence frequencies in the middle to upper TTL agree well with those based on satellite observations (spatial correlation of 0.8). Waves and convection enhance cloud occurrence at the cold point tropopause by 4% and 2%, respectively. Temporal variability of the heating rates as indicated by the ERA-Interim 6-hourly heating rate fields dehydrates the TTL by 0.4 ppmv and decreases the cloud occurrence by 4% because parcels are more likely to encounter the coldest temperatures and dehydrate near the cold point, limiting cloud formation above. The final dehydration locations of parcels, concentrated near the dateline in the tropical Pacific, are insensitive to various model parameters.

1. Introduction

The interplay of dynamical, radiative, chemical, and cloud microphysical processes determines the observed structure and unique properties of the tropical tropopause layer (TTL) [*Fueglistaler et al.*, 2009; *Randel and Jensen*, 2013, and references therein]. Since the TTL acts as a gateway to the stratosphere for atmospheric tracers such as water vapor (H_2O) [*Brewer*, 1949] and very short-lived substances, which play an important role in stratospheric ozone and climate [e.g., *Holton et al.*, 1995; *Solomon et al.*, 2010], understanding the impact of TTL processes on tracer transport is imperative for reliable future climate projections. Current global chemistry climate models are limited in their representation of key TTL processes [*Gettelman et al.*, 2009, 2010], including the detailed microphysics of TTL cirrus clouds that drive dehydration. Humidity and clouds are tightly coupled in the TTL, and thus, the modulation of TTL cirrus by those same processes can amplify the climate response through positive cloud feedback, which further underscores the importance of quantifying the roles of relevant TTL processes.

While the dominant role of tropical tropopause temperatures in regulating the amount of H_2O entering the stratosphere has been well established for some time [*Brewer*, 1949; *Mote et al.*, 1996; *Holton and Gettelman*, 2001], recent studies have shown that wave-driven temperature variability, convective influence, and cloud-related (microphysical, dynamical, and radiative) processes in the TTL have nonnegligible impacts on TTL humidity [*Gettelman et al.*, 2002a; *Bonazzola and Haynes*, 2004; *Jensen and Pfister*, 2004; *Schiller et al.*, 2009; *Liu et al.*, 2010; *Schoeberl and Dessler*, 2011; *Dinh and Fueglistaler*, 2014; *Schoeberl et al.*, 2014; *Ueyama et al.*, 2014]. Comprehensively, these studies have generally concluded that waves dehydrate, whereas convection and cloud (microphysics and cloud-induced heating) processes moisten the TTL. However, due to the modeling complexity and limitations in data availability and/or quality, existing studies on this topic have provided pieces of the puzzle, but not its entirety.

Here we revisit the study of *Jensen and Pfister* [2004] (hereafter denoted as JP), which examined the various controls on TTL dehydration in one-dimensional (vertical) time-dependent simulations of ice clouds along trajectories. Though certainly not without limitations (see discussion in section 4), this approach has the advantage of simulating realistic vertical transport of cloud particles, rather than specifying a characteristic removal timescale for simple microphysical box models. In this study, the dynamical, convective, and microphysical effects on TTL humidity and clouds during boreal winter 2006–2007 are examined using more reliable data sources (e.g., meteorological fields with wave-enhanced variability in the TTL) and improved methodology (e.g., modeling of the convective influence along trajectories), as described in section 2. The recent work of *Schoeberl et al*. [2014] investigated similar questions regarding the control of stratospheric H_2O and upper tropospheric clouds during 2008–2009 using a comparable but slightly different approach, as discussed in section 2. The H_2O field at the 100 hPa level on 1 February 2007 and cirrus cloud abundance in the TTL during December 2006 to January 2007 are simulated in our model and compared to observations in section 3. Sensitivity tests that exclude each of the three processes of interest—waves, convection, and cloud microphysical processes—are analyzed to quantify the effects of these processes on TTL humidity and clouds. The impact of the radiative heating rates used to calculate the diabatic trajectories is also highlighted. A summary of the results and a discussion of their implications on the long-term variability and trend in stratospheric H_2O are presented in section 4.

2. Data and Methods

Water vapor and cloud fields in the TTL are simulated in three steps: (i) calculate 60 day backward diabatic trajectories on isentropic coordinates launched once a day over a 7 day period centered on 1 February 2007 (i.e., a total of seven sets of trajectories ending on 29 January to 4 February 2007) from a 2° latitude × 2° longitude grid of points in the tropics (20°S–20°N) at 372 K potential temperature level (which corresponds to ~100 hPa level), (ii) simulate the evolution of ice clouds in one-dimensional (vertical) space along each trajectory path, (iii) compare simulated H_2O mixing ratios at 100 hPa on the final day (start of the backward trajectories; Day 0) and cloud abundance statistics averaged over the seven sets of trajectories with corresponding satellite observations.

This combined trajectory and cloud model approach generally follows the method described in detail in JP and has been evaluated in a case study by *Ueyama et al*. [2014]. Briefly, in step (ii), time-height "curtains" of temperature and heating rate (vertical wind for JP) are constructed by extracting their vertical profiles (350–430 K potential temperature levels) versus time (0–60 days) from their respective data sets (descriptions below). Cirrus cloud processes are simulated along the trajectory curtains using a Lagrangian cloud microphysical model initialized with observed H_2O profiles at the latitude-longitude grids on the earliest day (Day −60) of the trajectories. The model simulates homogeneous ice nucleation when the ice saturation ratio, calculated using the temperature curtains, exceeds a threshold of ~1.6 [*Koop et al*., 2000]; thousands of individual ice crystals are tracked, allowing for a proper representation of the ice size distribution. The heating rate curtains are used to diagnose the vertical (cross-isentropic) transport of ice crystals and H_2O through the depth of the TTL following the trajectory path, and thus, this approach properly treats the vertical redistribution of water by clouds. The model calculates vertical profiles of H_2O and clouds at each time step along the 60 day trajectories. In this study, we examine the simulated H_2O mixing ratios at 100 hPa level on the final day as well as the cloud occurrence frequencies as a function of potential temperature during the 60 day integration period. Integration lengths of 60 days were chosen to allow sufficient time for the dehydration processes to complete, as discussed in section 3.4. Notable improvements in the methodology and data sources from those of JP are described below.

Vertical motions of parcels along their diabatic trajectories are based on boreal winter 2006–2007 mean, offline calculations of tropical radiative heating rates of *Yang et al*. [2010] merged with extratropical radiative heating rates from Modern-Era Retrospective Analysis for Research and Applications (MERRA) [*Reinecker et al*., 2011] averaged over the same time period. *Yang et al*. [2010] heating rates, shown in Figure 1, are calculated using analysis temperatures, chemical constituents, and satellite cloud observations and therefore are likely to be more representative of reality than those derived from analysis models (see also *Randel and Jensen* [2013, Figure 3]) due to the difficulties of simulating clouds and convection in global models [e.g., *Schoeberl et al*., 2014]. Uncertainties in MERRA extratropical heating rates should not be of concern for this study since

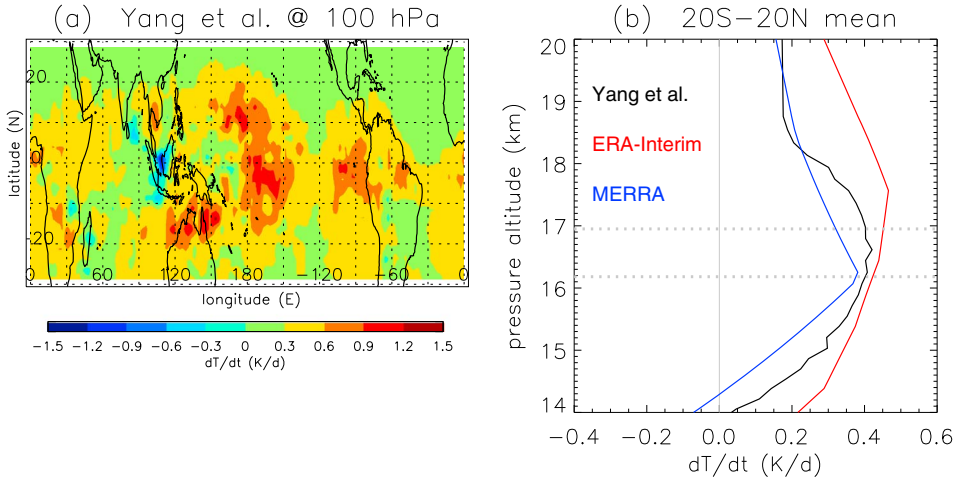

Figure 1. (a) The 100 hPa level boreal winter (December 2006 to February 2007) mean radiative heating rate (K d^{-1}) field in the tropics based on *Yang et al.* [2010] data derived from calculations using analysis temperatures, chemical constituents, and satellite cloud observations. (b) Vertical profiles of tropical (20°S–20°N) mean heating rates of *Yang et al.* [2010] (black), ERA-Interim (red), and MERRA (blue) reanalysis. Dotted horizontal lines in Figure 1b indicate the pressure altitudes corresponding to the cold point tropopause (17.0 km) and the 100 hPa level (16.2 km).

the trajectories are mainly confined equatorward of 30° such that the mean residence time of parcels in the tropics is 55.5 days (out of 60 days). A limitation of the *Yang et al.* [2010] data is their coarse (monthly) temporal resolution; we will assess the importance of the temporal variability of the heating rates in section 3.4.

In this study, temperatures from the 6-hourly interim reanalysis of the European Centre for Medium-range Weather Forecasts (ERA-Interim) [*Dee et al.*, 2011] are used, which avoids the need for the warm bias temperature correction in JP. The ERA-Interim cold temperature bias compared with radiosondes in the tropopause layer and the lower stratosphere was reduced after the assimilation of Global Positioning System radio occultation data, most notably since December 2006 [*Poli et al.*, 2010]. The agreement between ERA-Interim and aircraft measurements of TTL temperatures over the eastern tropical Pacific in boreal fall 2011 was verified in *Ueyama et al.* [2014]. Cold point temperatures in the tropics based on 6-hourly ERA-Interim data compare well with those of radiosondes for boreal winter 2006–2007 (see discussion in section 4), providing confidence in the use of ERA-Interim temperatures for this study.

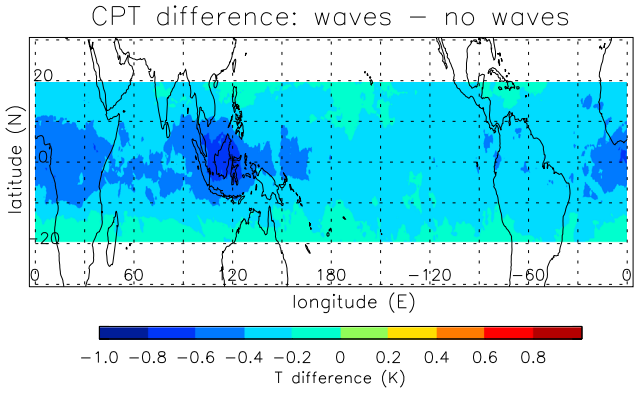

Figure 2. Boreal winter (December 2006 to February 2007) mean distribution of the tropical cold point tropopause temperature (K) effect of TTL waves recovered by the *Kim and Alexander* [2013] wave scheme which uses Fourier analysis to interpolate between vertical levels of ERA-Interim data and enhances the power at high frequencies to match the power spectrum obtained from tropical radiosonde data.

As noted by *Kim and Alexander* [2013], analyses are unable to capture all of the variability present in the TTL. The primary errors result from inadequate vertical resolution and suppressed variance at high frequencies. JP used a statistical representation of this "subgrid scale" variability to account for the effects of waves of all spectra. In contrast, we apply the wave scheme of *Kim and Alexander* [2013] that recovers the degraded wave-driven variability in the ERA-Interim data in the TTL. Instead of linear interpolation, the scheme properly interpolates between vertical levels using Fourier analysis and enhances the power at frequencies of ~0.1 to 2 cpd (or period^{-1}) to match the power spectrum obtained from tropical radiosonde data. The interpolation

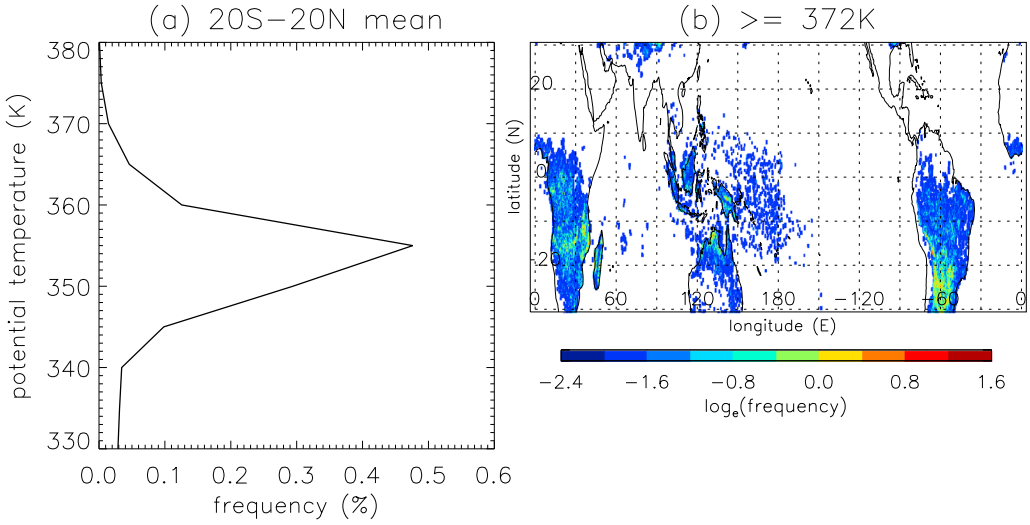

Figure 3. Boreal winter (December 2006 to February 2007) mean occurrence frequencies (%) of convective cloud top potential temperatures estimated from geostationary satellite imagery and rainfall measurements (see text for details): (a) tropical (20°S–20°N) mean profile and (b) distribution at and above the 372 K potential temperature (~100 hPa) level.

technique is applied to both the temperature and the horizontal wind data, but only the power of the temperature data is enhanced due to uncertainties in the power amplification factor for the wind fields.

Figure 2 shows the effect of the "subgrid-scale waves" (hereafter just "waves") on tropical cold point temperature during boreal winter 2006–2007. Waves decrease the average cold point temperature in the tropics by approximately 0.3 K (with a maximum decrease of 0.8 K over Indonesia); the cold temperature excursions in wave-driven temperature fluctuations will further dehydrate the TTL. This agrees well with the ~0.35 K reduction in the average cold point temperature using the same wave scheme on MERRA data between 2007 and 2013 documented by *Wang et al*. [2015]. High-frequency (>2 cpd) variability that is not resolvable in the wave scheme is added to the trajectory temperatures prior to running the cloud model following the statistical wave scheme described in JP. Note that large-scale waves, such as Kelvin waves with vertical wavelengths greater than ~4 km, are resolved in global reanalysis data and thus are present in all simulations (including those referred to as "simulation without waves").

A significant advancement from JP is the inclusion of the convective influence determined by tracing the trajectory paths through time-dependent (3-hourly) fields of convective cloud top height estimated from geostationary satellite imagery and rainfall measurements [*Pfister et al*., 2001; *Bergman et al*., 2012]. When a trajectory intersections a cloud, the atmospheric column at the parcel's location is saturated up to the cloud top altitude. Using this approach, *Ueyama et al*. [2014] showed that accurate (to within 0.5 to 1 ppmv) predictions of TTL humidity requires proper representation of convection, which predominantly hydrates the lower TTL by 1 to 5 ppmv. We use the same convection scheme here, except we apply distinct rainfall rate thresholds over land (9 mm h^{-1}) and ocean (1.5 mm h^{-1}), as opposed to a fixed rainfall threshold of 1 mm h^{-1}, to search for convective grid points. Figure 3 shows the frequency of convective cloud top altitude (in potential temperature coordinate) averaged over the tropics (20°S–20°N) during boreal winter 2006–2007. Convective clouds in the tropics typically peak at the 355 K (~150 hPa) level near the bottom of the TTL [*Gettelman et al*., 2002b; *Liu et al*., 2007; *Luo et al*., 2008]; most of these clouds are located over the Intertropical Convergence Zone and South Pacific Convergence Zone in the Pacific, north equatorial Atlantic, Indian Ocean, and the Maritime Continent (not shown). Only a small fraction (0.01%) of tropical convective clouds extend up to the 372 K (~100 hPa) level, primarily over land (e.g., South America, Southern Africa, Northern Australia, and Maritime Continent) and the western Pacific (Figure 3b), but their potentially large impact on TTL humidity and cirrus cloud occurrence is of interest to this study. We note that the convection scheme overestimates the cloud top altitudes northward of 30°N due to the excessively high convective plume equivalent potential temperatures at middle and high latitudes, but the effect of these deep clouds on TTL humidity and clouds is minimal (not shown).

The model is initialized with 7 day mean H_2O data from Microwave Limb Sounder (MLS) [*Read et al*., 2007] averaged over 5° latitude × 5° longitude bins, though the results of this study are not sensitive to the initial H_2O distribution, as discussed in section 3.4. The simulated H_2O mixing ratios on the final day of the trajectories (Day 0) spanning 29 January to 4 February 2007 are averaged and then compared with centered 7 day mean MLS H_2O data on 1 February 2007 at the 100 hPa level. The typical single-profile accuracy for H_2O at the 100 hPa level is 15% (~0.5 ppmv). MLS H_2O retrievals represent an average over 3–4 km layer atmosphere, and thus, proper vertical averaging of the model data is essential for a meaningful comparison with MLS data. Following the description of the averaging kernels for MLS version 3.3 profiles in the Data Quality and Description Documentation, model values at the MLS pressure levels are estimated using a linear least squares fit. The differences between the pressure level mixing ratios of the model and of the climatological mean MLS a priori are then convolved with the MLS averaging kernel. The result is added to the MLS a priori values in the final step.

In situ formed clouds in the one-dimensional, time-dependent cloud microphysical model, while not expected to match observations on a cloud by cloud basis, provide meaningful statistics of the seasonal mean TTL cirrus cloud abundance that can be compared with observations. The simulated cloud occurrence frequencies are compared with those estimated from Cloud-Aerosol Lidar and Infrared Pathfinder Satellite Observations (CALIPSO) [*Winker et al*., 2009]. The ice water content product and the vertical feature mask in Level 2 Cloud Profile data available at 5 km horizontal (along track) resolution and 60 m vertical resolution are used to calculate the cloud occurrence frequencies in the TTL averaged over 5° latitude × 5° longitude grid in the tropics from December 2006 to January 2007. The simulated and observed tropical mean cloud occurrence frequencies are compared at all TTL levels between 14 and 18 km, but the spatial correlation between the simulated and observed cloud occurrence patterns are evaluated using data in the middle to upper TTL (16–18 km) only. Model cloud statistics are particularly robust in the middle to upper TTL because the assumption of a simple isentropic flow with vertical motion balanced by radiative heating is a reasonable approximation at these levels. In the lower TTL at and above the model's bottom boundary, convective motions and latent heating complicates the balance. Additionally, convective detrainment will likely impact H_2O mixing ratios and cloud abundance in the lower TTL, but a realistic convective detrainment profile is not well known.

The methodology described above parallels that of *Schoeberl et al*. [2014] who also used a trajectory model combined with a cloud module and convection product to examine the effects of waves, cloud microphysical processes, and convection on TTL water and clouds. Our study differs from that of *Schoeberl et al*. [2014] in five aspects: First, we calculate backward trajectories from a grid of points at the 372 K potential temperature level (instead of the domain-filling, forward trajectory approach that tracks more numerous parcels). Second, we use time-independent, offline calculations of (instead of time-dependent, model-derived) TTL radiative heating rates to calculate the diabatic trajectories. Third, we apply the *Kim and Alexander* [2013] wave scheme to ERA-Interim temperature *and wind* data (rather than to MERRA temperatures only). Fourth, we quantify the convective influence of air parcels by comparing the trajectory locations and times with time-varying, observation-based estimates of convective cloud top altitudes (instead of using the MERRA anvil ice product). Fifth, our one-dimensional cloud model properly treats the vertical transport of ice and water throughout the depth of the TTL (in contrast to the zero-dimensional parcel model whose ice sedimentation rate depends on an assumed cloud thickness). Our cloud model also calculates the size distribution of ice crystals within each grid box by tracking the size and height of individual ice crystals (instead of assuming a monodispersed ice crystal size distribution) and calculates the ice nucleation rates at each location and time step that are used to properly deplete the aerosol population (instead of using an ice nucleation scheme that depends on model cooling rate and temperature). Despite these differences, we will show in the next section that our results are in reasonable agreement with those of *Schoeberl et al*. [2014].

3. Results

3.1. H_2O Mixing Ratio at 100 hPa

The 100 hPa H_2O field as measured by MLS during boreal winter 2006–2007 is shown with colored shading in Figure 4. A sharp meridional gradient at ~30°N/S clearly separates the dry tropical air (30°S–30°N mean of 3.7 ppmv) from the moist extratropical air (30°N/S–60°N/S mean of 4.2 ppmv), but moist air intrusions from

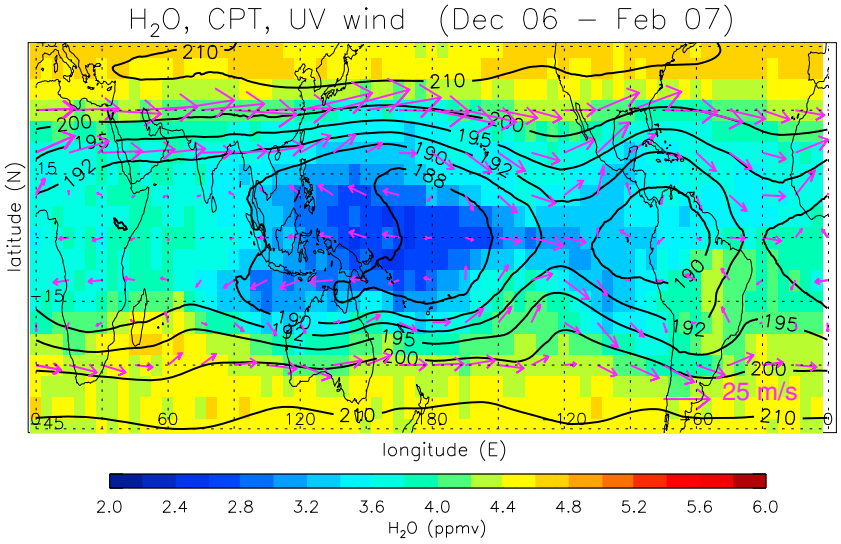

Figure 4. The 100 hPa level boreal winter (December 2006 to February 2007) mean H_2O mixing ratios (ppmv; color shading) from MLS data superimposed with ERA-Interim cold point tropopause temperature (K; contours) and 100 hPa horizontal wind ($m\,s^{-1}$; vectors) fields.

the extratropics are observed regionally following the meridional wind flow (e.g., along 120°W, 30°W, and 60°E). The pattern in the tropics consists of a prominent dry region over the western tropical Pacific and a weaker dry region over the eastern tropical Pacific, roughly coincident with the cold point tropopause temperature field shown in contours.

The centered 7 day mean MLS H_2O field at the 100 hPa level equatorward of 20°N/S on 1 February 2007, shown in Figure 5b, exhibits the same basic features of the seasonal mean pattern (Figure 4) but with a seasonal minimum tropical mean H_2O mixing ratio of 3.1 ppmv. Figure 5a shows the simulated H_2O field at the 100 hPa level on the final day of the trajectories, calculated using the MLS averaging kernel as described above, averaged over all seven sets of trajectories ending 29 January to 4 February 2007. The simulated field

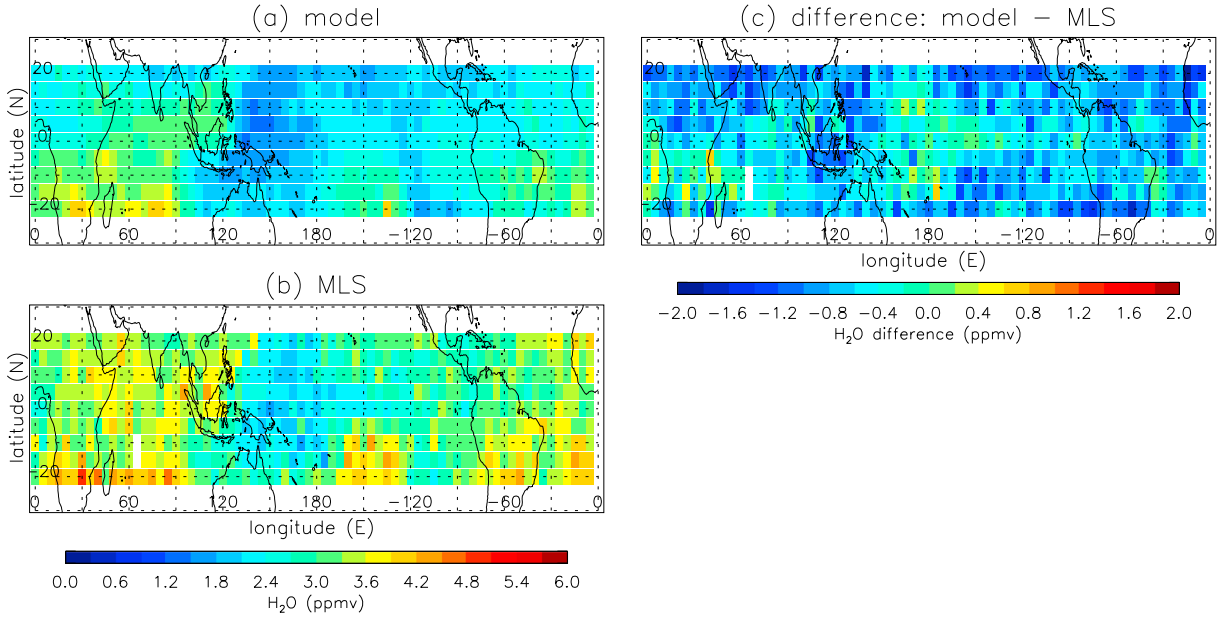

Figure 5. The 7 day (29 January to 4 February 2007) mean H_2O mixing ratios centered on 1 February 2007 at the 100 hPa level in the tropics as (a) simulated in the model, (b) observed by MLS, and (c) the difference (Figure 5a – Figure 5b) field. Tropical mean values are 2.4 (Figure 5a), 3.1 (Figure 5b), and –0.7 ppmv (Figure 5c).

generally resembles the observed field with a statistically significant (at the 99% level) spatial correlation (r) of 0.73 and root-mean-squared error (RMSE) of 0.35 ppmv. The western Pacific is anomalously dry, as in observations, but the driest air is centered at 130°–150°E, shifted westward from the observed minima at ~150°E–180°. The secondary dry region over the eastern Pacific appears as a distinct meridional corridor of dry air along 120°W longitude. The moist intrusions from the extratropics evident in Figure 5b near the southern tropical border between 160° and 120°W are not as clear in the model. The difference field shown in Figure 5c indicates that the simulated field is drier than observations throughout most of the tropics (tropical mean difference of −0.7 ppmv), except over the western and central Pacific where the cold point temperature dips below 188 K (Figure 4). The dry bias tends to be concentrated along the northern and southern tropical border ~20°S/N. Possible causes of the model dry bias of 0.7 ppmv, including the roles of small-scale mixing and detrainment of ice from deep convection, are explored in sections 3.3 and 4.

3.2. TTL Cloud Abundance

CALIPSO profiles during December 2006 and January 2007 are scanned for features identified as clouds. The cloud counts are used to calculate cloud occurrence frequencies in the TTL, which are compared with model cloud statistics over the same region and time period. Similar results are obtained using January 2007 data only.

The vertical profile of tropical (20°S–20°N) mean cloud occurrence frequency from CALIPSO measurements, shown in Figure 6a, indicates that cloud occurrence decreases rapidly with height above a pressure altitude of ~15 km: During these two months, clouds are present one fourth to one third of the time in the lower TTL below 16 km (~100 hPa), diminishing to less than one tenth of the time (9%) near the cold point at 17 km. As seen in Figure 7b, clouds in the 16–18 km layer are mainly concentrated over the western and central Pacific and Northern Australia, and to a lesser extent over the eastern Pacific, Southern Africa, and South America.

Cloud occurrence frequencies in the model agree remarkably well with observations at and above the cold point, where the tropical mean profiles agree to within a few percentages (Figure 6b). On average, the model overestimates cloud abundance below the cold point by approximately 5% compared to CALIPSO estimates. Despite the overestimation of lower to middle TTL clouds, the tropical mean cloud occurrence frequency in the 16–18 km layer (12%) is comparable to observations (9%) and the cloud distributions are well correlated with observations at $r = 0.82$ (RMSE of 5.5%) at the 99% significance level (Figures 7a and 7b). The dipole structures in the difference field (e.g., east-west dipole about the 165°E longitude over the central Pacific and north-south dipole over Africa in Figure 7c) suggest that much of the discrepancy is associated with shifts in the cloud locations.

Given that the TTL clouds are well simulated in our model, we further investigate the locations of final dehydration or rehydration of the parcels, shown in Figure 8. Final dehydration or rehydration is defined as the final in situ cloud formation or convective influence along a trajectory, whichever is later in time. Typically (~95% of the time), final in situ cloud formation occurs *after* the final convective rehydration event along a given trajectory, and thus Figure 8 may be interpreted (and hereafter referred to) as the final dehydration locations of parcels, which most frequently occur over the tropical Pacific centered on the dateline. Final dehydration locations generally follow the cold point temperature distribution (Figure 4), consistent with the notion that a parcel's humidity is primarily set during its passage through the cold point tropopause. On average, the final dehydration of parcels ending at the 100 hPa level occurs at an altitude of approximately 16.5 km, between the cold point tropopause and the 100 hPa level, as shown in Figure 8b.

3.3. Effects of Waves, Convection, and Microphysics

The sensitivities of the 100 hPa H_2O mixing ratios and TTL cloud occurrence frequencies to (i) waves, (ii) convective influence of parcels along their trajectories, and (iii) detailed microphysical processes such as ice nucleation, deposition growth, sedimentation, and sublimation are investigated by excluding each of these processes in the model simulations. We use only one set of trajectories ending at 1 February 2007 for all sensitivity tests, including those discussed in the following section 3.4, and the simulations are compared with the "base" simulation (which includes all three processes) on the corresponding date. We note that the results are not sensitive to ± few Kelvin difference in the potential temperature level from which the parcel trajectories are launched. Table 1 summarizes the sensitivities of the tropical (20°S–20°N) mean 100 hPa H_2O mixing ratio and cloud occurrence frequency in the middle to upper TTL to each of the variables, presented as

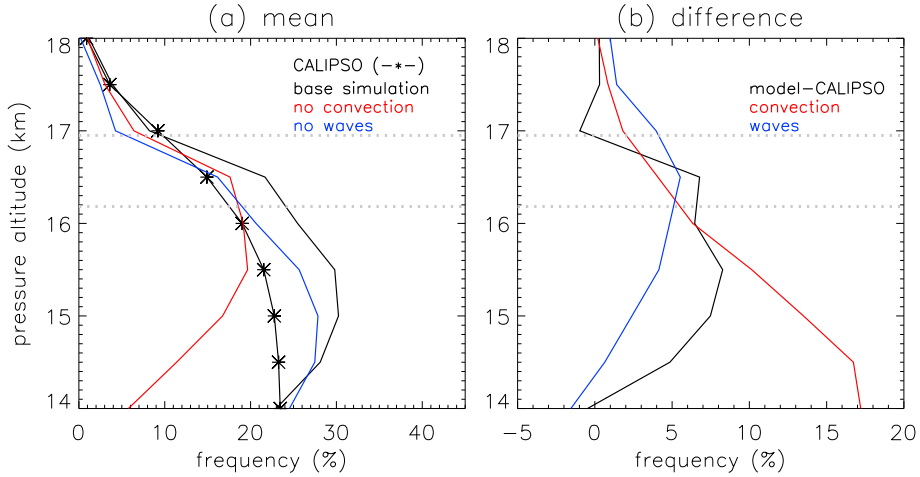

Figure 6. Vertical profiles of the tropical (20°S–20°N) mean cloud occurrence frequencies during boreal winter (December 2006 to January 2007) as observed by CALIPSO (asterisks) and in the model simulations. Base simulation (black) includes both convection and waves, while "no convection" (red) and "no waves" (blue) simulations exclude each of these processes. (b) Vertical profiles of the cloud occurrence frequency difference relative to the base simulation (i.e., "base simulation" minus CALIPSO (black), no convection (red), no waves (blue)). Dotted horizontal lines indicate the pressure altitudes corresponding to the cold point tropopause (17.0 km) and the 100 hPa level (16.2 km).

differences from the base simulation values (2.46 ppmv and 12.3%, respectively). The horizontal distribution of final dehydration locations (Figure 8a) is not sensitive to these TTL processes and therefore not shown.

3.3.1. Waves

To examine the effect of waves on TTL processes, the model is run using the standard 60 model level ERA-Interim temperatures and winds without the *Kim and Alexander* [2013] wave scheme. The resolved large-scale waves and the statistically represented high-frequency (>2 cpd) gravity waves are still present in this simulation.

The 100 hPa H_2O field in the simulation without waves, shown in Figure 9a, exhibits a similar pattern as those of the MLS observation and the base simulation (Figures 5a and 5b). Wet and dry features are more accentuated in

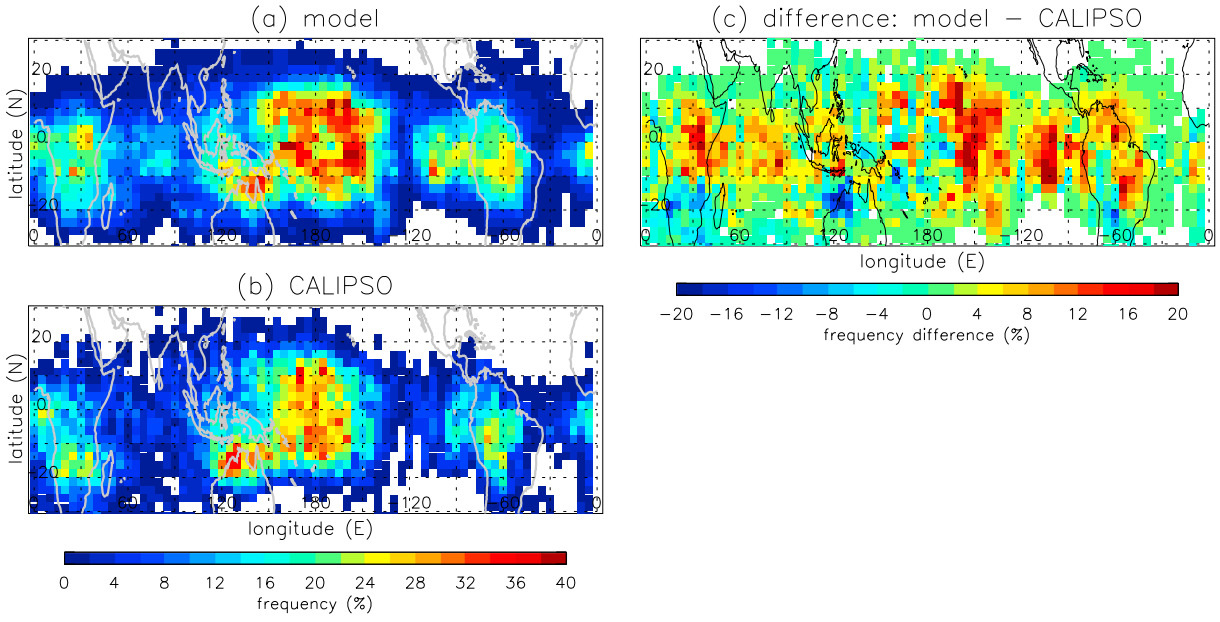

Figure 7. Boreal winter (December 2006 to January 2007) mean cloud occurrence frequencies (%) between 16 and 18 km pressure altitudes as (a) simulated in the model, (b) observed by CALIPSO, and (c) the difference (Figure 7a − Figure 7b) field. Tropical mean values are 12 (Figure 7a), 9 (Figure 7b), and +3% (Figure 7c).

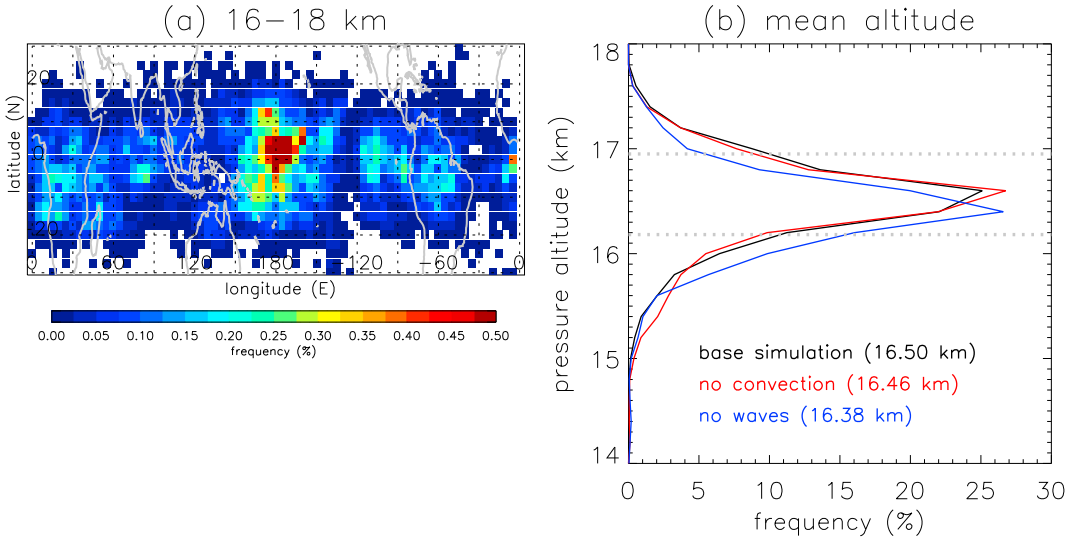

Figure 8. (a) Boreal winter (December 2006 to January 2007) mean final cloud occurrence frequencies (%) between 16 and 18 km pressure altitudes, defined as the location of final in situ cloud formation or convective influence along a trajectory, whichever is later in time. (b) Final cloud occurrence frequencies (%) as a function of pressure altitude (mean altitudes in parenthesis) in the base simulation (black) and in the simulations that exclude convection (red) and waves (blue). Dotted horizontal lines in Figure 8b indicate the pressure altitudes corresponding to the cold point tropopause (17.0 km) and the 100 hPa level (16.2 km).

Table 1. The Sensitivities of the Tropical (20°S–20°N) Mean 100 hPa H_2O Mixing Ratio and Cloud Occurrence Frequency in the Middle to Upper TTL to Each of the Variables, Presented as Differences From the Base Simulation Values[a]

	H_2O (ppmv)	Cloud Occurrence Frequency (%)
Base simulation (with waves, convection, microphysics)	2.46	12.3%
Waves	−0.46	+3.6
High-frequency (>2 cpd) waves	−0.08	+2.0
Convection	+0.34	+2.9
Convective ice injection	+0.55	+12
High (>370 K) clouds	+0.09	+0.86
Microphysics (homogeneous nucleation only)	+0.71	N/A
Heterogeneous nucleation	−0.05	+2.5
Homogeneous nucleation threshold (ice saturation ratio = 1.3 to 1.6)	+0.02	−4.0
Trajectory length (30 day instead of 60 day trajectory)	+2.13	−3.6
Initial H_2O (zonal mean MLS H_2O)	0.00	+0.01
ERA-Interim radiative heating rates (instead of *Yang et al.* [2010] data)	+0.47	+5.1
Temporal variability of heating rates	−0.39	−3.9

[a](top row) The tropical (20°S–20°N) mean H_2O mixing ratios (ppmv) at the 100 hPa level on 1 February 2007 and cloud occurrence frequency (%) in the 16–18 km layer during December 2006 to January 2007 of the base simulation. (rows 2–13) Sensitivities of the H_2O mixing ratio and cloud occurrence frequency (as differences from the base simulation values) to the various parameters. The impacts of "waves," "convection," and "microphysics" are calculated as the difference between the base simulation and the "no waves," "no convection," and "no microphysics" simulations, respectively. Waves with frequencies higher than 2 cpd are omitted to quantify the impact of "high-frequency waves." Ice crystals are added uniformly up to the cloud top altitude in "convective ice injection" simulation. The difference between the base simulation and the simulation with convective cloud top potential temperatures capped at 370 K is used to quantify the impact of "high clouds." Heterogeneous freezing of parcels is allowed in the simulation used to quantify the impact of "heterogeneous nucleation." "Homogeneous nucleation threshold" is lowered from 1.6 (base simulation) to 1.3. The integration lengths of 30 days (instead of 60 days of the base simulation) are used to examine the sensitivity to the "trajectory length"; cloud occurrence frequencies in January 2007 are used for the comparison. The model is initialized with zonal mean MLS H_2O mixing ratios to examine the sensitivity to "initial H_2O" conditions. Simulation using seasonal mean "ERA-Interim radiative heating rates" is compared with the base simulation using seasonal mean, observation-based *Yang et al.* [2010] heating rates. Simulations with seasonal mean and 6-hourly ERA-Interim heating rates are compared to quantify the impact of the "temporal variability of the heating rates."

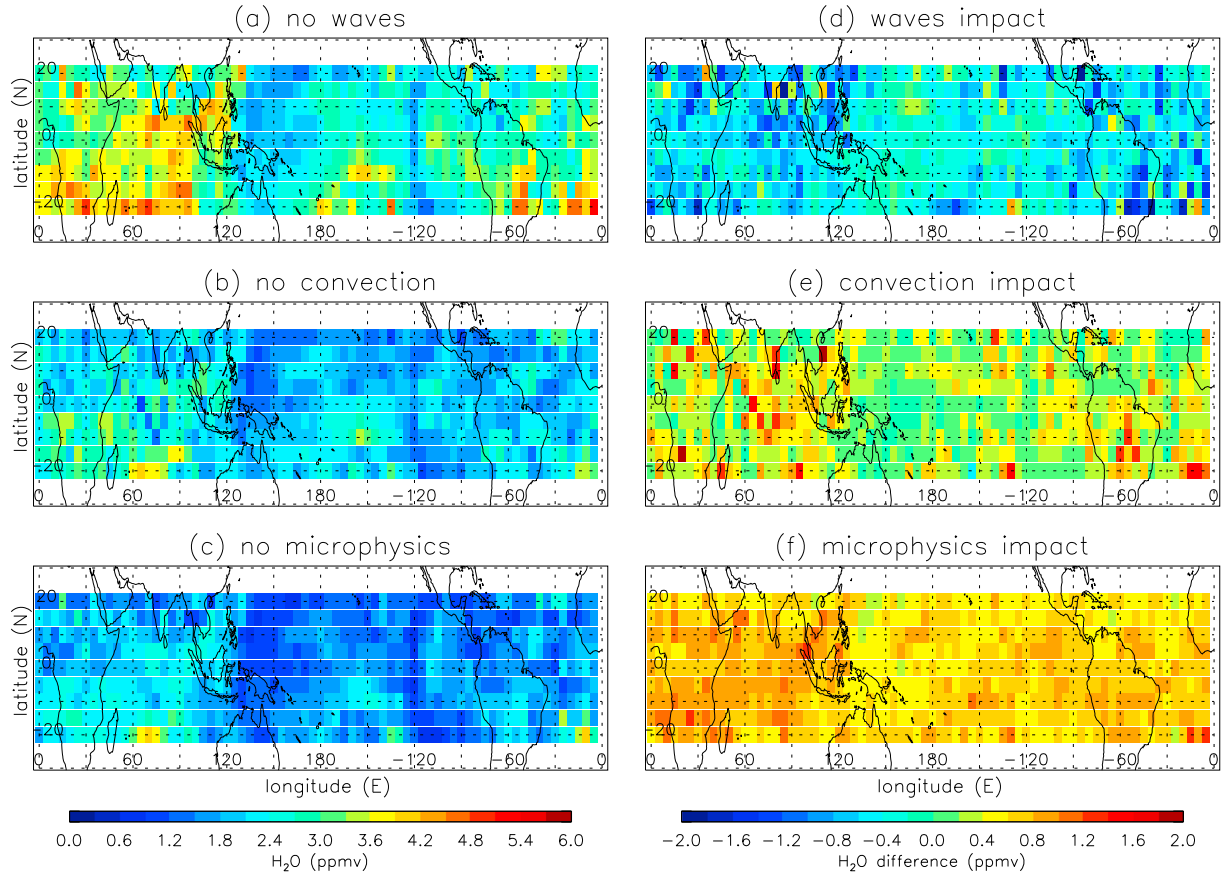

Figure 9. (a–c) The 100 hPa level H_2O mixing ratios and (d–f) difference fields between sensitivity test simulations and the base simulation on 1 February 2007. Tropical mean values are 2.9 (Figure 9a), 2.1 (Figure 9b), and 1.7 ppmv (Figure 9c). The impacts of waves (Figure 9d), convection (Figure 9e), and microphysics (Figure 9f) on the 100 hPa H_2O mixing ratios.

Figure 9a compared to observations, resulting in a tropical mean H_2O mixing ratio of 2.9 ppmv. The 100 hPa level is more moist without waves when compared to the base simulation. Indeed, the difference field of the simulated H_2O with and without waves in Figure 9d indicates that waves dehydrate the 100 hPa level by ~0.5 ppmv in the tropical mean (Table 1), consistent with the results of JP and *Ueyama et al.* [2014] and slightly greater than the estimates of *Schoeberl et al.* [2014] (0.2 ppmv) and *Wang et al.* [2015] (0.3 ppmv). Dehydration is especially prominent over Indonesia, which resembles the pattern of the cold point temperature change due to waves in Figure 2. Waves lower the cold point temperature, thereby increasing the dehydration of air parcels during their ascent through the TTL.

Waves also enhance cloud occurrence throughout the depth of the TTL, as shown in Figure 6; cloud occurrence frequency is enhanced by 4% at the cold point tropopause. Waves not only raise the final dehydration altitude by ~0.1 km (Figure 8b), but their dehydration efficiency is maximized near the cold point tropopause because the wave-induced temperature decrease at the cold point has a greater impact on dehydration and cloud formation than a temperature change of the same magnitude in the warmer, lower TTL. Figure 10a shows the distribution of cloud occurrence frequencies in the 16 to 18 km layer in the simulation without waves. Frequencies are lower than those of the base simulation (Figure 7a), but the spatial correlation with CALIPSO observations (Figure 7b) remains high ($r = 0.76$), suggesting that waves do not significantly influence the latitudinal and longitudinal locations of middle to upper TTL cloud formation. Waves do, however, improve the spatial bias in the low cloud occurrence frequency in the southern tropics between 120°E and 170°W in Figure 10a compared to CALIPSO observations in Figure 7b. As evident in Figure 10c, wave-driven enhancement of clouds generally occurs where clouds prevail in the time mean (Figure 10a).

Waves of different frequencies and wavelengths have variable effects on TTL properties. Here we investigate the role of high-frequency (>2 cpd) waves by excluding the statistically represented gravity waves beyond

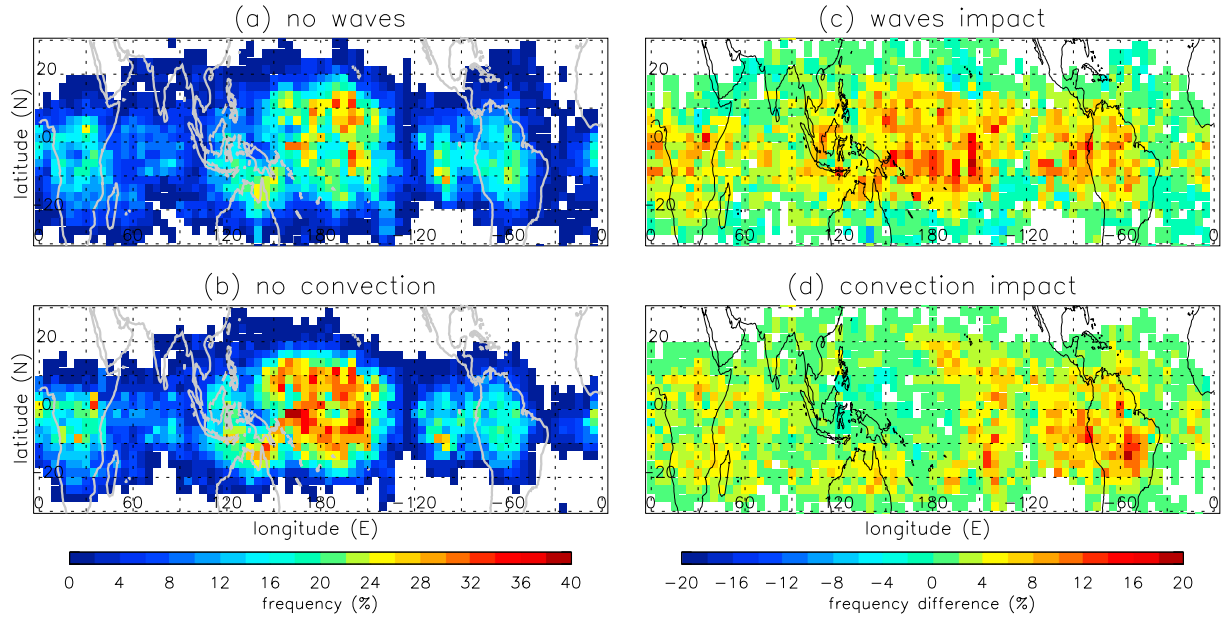

Figure 10. Boreal winter (December 2006 to January 2007) mean cloud occurrence frequencies (%) between 16 and 18 km pressure altitudes in the model that excludes (a) waves and (b) convection. Tropical mean values are 8.7 (Figure 10a) and 9.4% (Figure 10b). The impacts of (c) waves and (d) convection on the cloud occurrence frequencies are calculated as the difference from the base simulation which includes both processes.

the frequencies resolvable in the *Kim and Alexander* [2013] wave scheme. The results in Table 1 indicate that high-frequency waves have an insignificant effect on TTL humidity (−0.08 ppmv) and clouds (+2.0%). This is consistent with the findings of *Fueglistaler and Baker* [2006] and *Schoeberl et al.* [2014] which show that the dehydration efficiency decreases with increasing frequency of the temperature oscillation because smaller ice crystals fall slower thus enhancing the likelihood of sublimation of ice crystals and remoistening of the TTL. However, high-frequency waves are expected to impact cloud microphysical properties such as ice number concentrations and ice crystal size distributions, which is beyond the scope of this study.

3.3.2. Convection

A simulation without the convection scheme (i.e., without saturating the air column up to the cloud top altitude), comparable to the baseline simulation of JP, is run to investigate the role of convection on TTL humidity and clouds. Figure 9b shows the excessively dry 100 hPa H_2O field with a tropical mean H_2O mixing ratio of 2.1 ppmv. The difference field in Figure 9e confirms that convection predominantly hydrates the 100 hPa level by approximately 0.3 ppmv, in general agreement with the results of *Schoeberl et al.* [2014] and *Ueyama et al.* [2014]. However, increases in H_2O due to convection (Figure 9e) do not necessarily coincide with regions of deep convection (Figure 3b). The effect of convection on H_2O is clearly minimal in regions where both the model and the CALIPSO measurements show significant cloud (implying high relative humidity), which are, for the most part, the coldest areas. In these regions, cold temperatures efficiently dehydrate the convectively injected H_2O through the freeze-drying process.

Convective enhancements of H_2O over Southern Africa and South America are due to direct injection into relatively warm (and dry) air, and the south Atlantic enhancement is due to the advection of injected African air by the mean easterly flow (Figure 4). Dehydration of convectively injected air from the western part of the Maritime Continent is inefficient due to the displacement of convection westward of the coldest temperatures. The injected water can then be advected westward by the prevailing easterlies into regions of even warmer temperatures and even less effective dehydration (e.g., Indian Ocean), continuing into northern Africa around the broad anticyclonic circulation north of the equator. Thus, the overall pattern of convective influence in Figure 9e reflects the moistening of the relatively warm regions of the TTL. Without convection, the flushing of air through the coldest regions results in an almost uniformly dry TTL, interrupted only by the injection of moist air from southern midlatitude troughs (Figure 9b).

The formation of in situ clouds at and downstream (along trajectory) of convection greatly enhances cloud occurrence in the lower TTL by up to 17% (at 14 km; Figure 6b). At and above the cold point tropopause,

convection has minimal effect on clouds (~1%). Regional differences in cloudiness due to convection (Figure 10d) do not always coincide with actual convective injection (Figure 3b), with the exception over east central South America. Typically, convectively induced increases in cloudiness occur at the edges of the cold regions: the western Pacific/Maritime Continent (enhancements over Northern Australia, and the north and south central Pacific), and the eastern Pacific/South America (enhancements over east central South America and the far eastern Pacific). Increases over Africa are relatively small; even though there is significant convection, temperatures are not very cold (Figure 4) so convection mainly enhances water (Figure 9e) but not clouds. The regions of enhanced cloud south of the equator near 140°W and 90°W are due to convective injection from the eastern portions of the South Pacific Convergence Zone (SPCZ). Injected vapor advected eastward from the SPCZ is nucleated at the edge of the southeastern portion of the western Pacific cold pool, and then again at the southwestern edge of the eastern Pacific cold pool (Figure 4). The enhancement in cloud southwest of Hawaii is due to injected vapor from convection in the South China Sea going around the anticyclone and recondensing as it moves southward into the cold region near the dateline. This phenomenon has been verified by aircraft measurements [*Pfister et al*., 2001]. Though convectively lofted H_2O in the coldest regions is efficiently nucleated and removed, cloud incidence is already high (Figure 10b); clouds may be thicker in those regions with convection included, but not necessarily more frequent.

It is notable that convection *decreases* both H_2O and cloud incidence near the center of the western Pacific cold pool. Because of the in situ ice nucleation threshold of ~1.6 (see section 3.3.3), supersaturation is a frequent occurrence in this cold region. Convection, by providing ready ice nuclei, quenches the supersaturation and effectively removes water. This dehydrating effect results in a lower incidence of in situ formed clouds by reducing relative humidity.

Convective lofting of ice crystals may provide another means of vertical transport of H_2O and influence TTL cloud formation. To examine this effect, ice crystals are added uniformly up to the cloud top altitude at every convection encounter along the trajectories. Previous measurements in convectively generated anvil cirrus at lower altitudes (12–13 km) indicated ice crystal diameters and number concentrations of ~60 μm and 100 L^{-1}, respectively [*Jensen et al*., 2009]. However, ice detraining in the higher, colder TTL will likely have more numerous, smaller ice crystals [*Knollenberg et al*., 1993; *Jensen and Ackerman*, 2006]. We assume a diameter of 20 μm and a concentration of 300 L^{-1} for ice detrained in the TTL. Using larger ice crystal sizes would result in faster sedimentation and decrease the impact of detrained ice on TTL H_2O and cirrus.

Convectively injected ice moistens the 100 hPa level by 0.5 to 0.6 ppmv (Table 1). The spatial distribution of its effect (not shown) resembles the pattern of the model dry bias in Figure 5c but with opposite sign, where regions outside of the western Pacific cold pool are substantially moistened. While the lack of convective ice in the base simulation may in part explain the model dry bias compared to MLS, convective ice injection increases the cloud occurrence frequency in the middle to upper TTL by 12% (Table 1), which is approximately 3 times more than observed by CALIPSO (25% versus 9%). The enhancement in cloud occurrence frequency in the lower TTL (not shown) may be associated with increased amounts of fallen ice crystals from deep convective cloud tops. The impact of convectively injected ice on TTL humidity and clouds estimated by *Schoeberl et al*. [2014] using a zero-dimensional parcel model with MERRA anvil ice product is slightly lower than our estimates.

Convective cloud tops that penetrate above the 370 K level are rare (Figure 3) but can potentially have a disproportionately large effect on TTL humidity and clouds. To isolate the impact of high (cloud top potential temperature $>$ 370 K) clouds, we calculated the difference between the base simulation and the simulation with convective cloud top potential temperatures capped at 370 K. The high clouds moisten the 100 hPa level by $<$0.1 ppmv and enhance the cloud occurrence by $<$1% (Table 1). The spatial pattern of the 100 hPa H_2O field (not shown) exhibits convective moistening outside of the western Pacific cold pool region and does not resemble the cloud top distribution in Figure 3b (with the exception of slight enhancements in humidity and clouds over the deep convective regions of South America), suggesting that the impact of deep convection on TTL humidity is mostly remote. In general, our results do not provide strong evidence for the importance of deep convection with cloud top potential temperatures above 370 K on TTL humidity and clouds.

3.3.3. Microphysics

Simple trajectory studies that assume instant removal of H_2O exceeding saturation without detailed microphysical processes have been shown to yield parcels that are too dry [e.g., *Liu et al*., 2010; *Schoeberl et al*.,

2014]. Here we examine the effect of cloud microphysical processes involving homogeneous ice nucleation of parcels exceeding an ice saturation ratio of approximately 1.6 [*Koop et al*., 2000] and subsequent deposition growth, sedimentation, and sublimation of ice crystals. In agreement with previous studies, the tropical average 100 hPa H_2O mixing ratio of the simulation without microphysics, shown in Figure 9c, is about half of the observed values (Figure 5b). While an average moistening of 0.7 ppmv occurs uniformly throughout the tropics, as evident in Figure 9f, the impact is minimal to the west of the Maritime Continent, presumably because air parcels over this region spiral around the anticyclone (Figure 4) for a sufficiently long time such that vapor in excess of ice saturation is effectively depleted by ice growth and all ice crystals eventually sediment out of the TTL by the time parcels ascend to the 100 hPa level.

The moistening by microphysical processes in our model can be attributed to three factors: (i) allowing for supersaturation with ice saturation ratio threshold of ~1.6 [*Koop et al*., 2000], (ii) only partial removal of vapor in excess of saturation by crystal deposition growth, and (iii) retaining H_2O in the form of ice which may sublimate below the initial cloud formation layer and rehydrate the atmosphere below. The relative importance of the first effect is investigated by running a simulation with lower ice saturation ratio threshold of ~1.3. As indicated in Table 1, increasing the supersaturation from 1.3 to 1.6 has a minimal effect on the 100 hPa level humidity. However, a higher supersaturation threshold in the base simulation decreases the cloud occurrence frequency by 4% because ice crystals do not nucleate until the atmosphere exceeds an ice saturation ratio threshold of ~1.6, which occurs less frequently than an ice saturation ratio of ~1.3. The relative importance of the supersaturation effect is greater in the simpler cloud model of *Schoeberl et al*. [2014] that excludes the moistening below the initial cloud formation layer in factor (iii).

Aircraft measurements suggest that homogeneous nucleation is prevalent in the TTL [e.g., *Jensen et al*., 2013], but the relative importance of heterogeneous nucleation is not known. *Froyd et al*. [2009] analyzed TTL aerosol composition data measured by an aircraft and showed the lack of evidence for heterogeneous freezing of ice crystals, while *Cziczo et al*. [2013] argued that heterogeneous freezing is the dominant formation mechanism of cirrus clouds in general. The effect of heterogeneous freezing of ice crystals on TTL H_2O and clouds are examined by comparing the results of a simulation with both homogeneous and heterogeneous nucleation schemes to those of the base simulation (homogeneous nucleation only). In addition to the abundant aqueous sulfate aerosols onto which homogeneous freezing takes place when parcels exceed an ice saturation ratio of ~1.6, a limited number (30 L^{-1}) of particles with solid inclusions are added to the model to allow for heterogeneous freezing of parcels at a lower supersaturation threshold of ~1.3. If cooling is strong enough, the number of heterogeneous nuclei will be insufficient to quench the rising supersaturation, and homogeneous freezing may ultimately be triggered. Our results show that the tropical mean H_2O mixing ratio at the 100 hPa level is virtually unaffected by heterogeneous ice nucleation (−0.05 ppmv), but the cloud occurrence frequency is enhanced by 2–3% in the middle to upper TTL because clouds are permitted to form at a lower supersaturation threshold (Table 1). Both homogeneous and heterogeneous freezing processes presumably occur to some degree in the real atmosphere. However, more observations are needed to constrain the amount and types of ice nuclei in the TTL to better quantify the relative roles of the two nucleation schemes on TTL humidity and cloud in our model.

3.4. Sensitivities to Other Processes

Uncertainties in trajectory paths grow exponentially with time and thus a single trajectory of this (60 days) length yields very little useful information. On the other hand, trajectories must be long enough for parcels to encounter the cold temperatures. Parcel locations at Day −30 are presumably known with higher certainty than those at Day −60, but a simulation with 30 day backward trajectories yields a tropical mean 100 hPa H_2O mixing ratio that is much too wet (Table 1) because many of the parcels have not had sufficient time for complete dehydration; without the passage through the cold temperature regions over the tropical Pacific during the parcel's slow ascent, the simulated H_2O at the 100 hPa level on Day 0 of the 30 day trajectory simulation reflects the initialized MLS H_2O mixing ratio at the parcel location on Day −30, which is relatively moist due to the parcel's lower altitude. One way to assess the impact of trajectory error is by examining the sensitivity of the results to the initial H_2O profiles at parcel locations on Day −60. The sensitivity test simulation is initialized with a zonal mean H_2O field from MLS data. As evident in Table 1, both the 100 hPa H_2O and the cloud occurrence frequency are insensitive to the initial conditions. Errors in the trajectory path and therefore in the temperature history along the trajectories will affect the cloud evolution and dehydration of individual parcels.

Nonetheless, statistically meaningful results can be attained with sufficient averaging of thousands of trajectories as done here. Thus, errors arising from uncertainties in trajectory paths should not be of great concern when interpreting these simulation results. We also note that the model cloud statistics for January 2007 are similar to the December 2006 to January 2007 statistics presented in this study and compare favorably to January 2007 CALIPSO measurements (not shown).

More importantly, TTL water and clouds appear to be sensitive to the radiative heating rates used to calculate the diabatic trajectories. *Wang et al*. [2014] have shown that the diabatic heating rates in the tropics are vastly different between various reanalyses (their Figure 1), which impact the vertical transport rate and concentration of tracers in the TTL. The seasonal mean radiative heating rates in the tropics (20°S–20°N) from ERA-Interim are only 5–10% larger than those of *Yang et al*. [2010] near the 100 hPa level, but the excessive ERA-Interim heating rates extend throughout the TTL (Figure 1b). As a result, the tropical mean H_2O mixing ratio calculated using ERA-Interim heating rates is larger than that based on *Yang et al*. [2010] heating rates by nearly 0.5 ppmv (Table 1). The ~20% increase in 100 hPa H_2O using the slightly larger ERA-Interim heating rates is a result of the reduced likelihood of parcels encountering the coldest temperature at the cold point altitude due to their faster ascent through the cold temperature regions, in agreement with *Schoeberl et al*. [2013]. This results in a moister TTL, which in turn leads to ~5% greater cloud occurrence in the middle to upper TTL (Table 1).

Simulation results using 3 month mean versus 6-hourly ERA-Interim heating rates are compared to assess the importance of the temporal variability of the heating rates on TTL water and clouds. As indicated in Table 1, heating rate variability dehydrates the 100 hPa H_2O by approximately 0.4 ppmv and decreases the cloud occurrence by ~4%. Parcels calculated using the variable heating rates potentially encounter the coldest temperatures at a higher altitude near the cold point tropopause, allowing for more dehydration and limiting cloud formation above the cold point. It is notable that the horizontal distribution of final cloud locations (Figure 8a) is neither sensitive to the choice of the heating rate data nor to the temporal variability (not shown).

4. Summary of Findings and Discussion

Processes that control the humidity and cloud abundance in the TTL during boreal winter 2006–2007 are investigated in simulations of clouds along parcel trajectories. Backward trajectories from the 372 K potential temperature (~100 hPa) surface in the tropics (20°S–20°N) are calculated using offline calculations of seasonal mean tropical radiative heating rates [*Yang et al*., 2010] and 6-hourly ERA-Interim reanalysis temperatures and winds with enhanced wave-driven variability [*Kim and Alexander*, 2013]. A one-dimensional (vertical), time-dependent cloud microphysical model is used to simulate the nucleation, deposition growth, sedimentation, and sublimation of in situ cirrus clouds and their effects on the humidity profile along the trajectory paths. We consider the convective influence of parcels whose trajectory path intersects with convective clouds detected in 3-hourly geostationary satellite imagery.

The simulated H_2O field on 1 February 2007 at the 100 hPa level, after appropriately applying the MLS averaging kernel, resembles MLS observations (spatial correlation $r = 0.73$), but exhibits a 0.7 ppmv dry bias in the tropical mean (Figure 5). Simulations that exclude waves, convection, and microphysics show that waves dehydrate the 100 hPa level by 0.5 ppmv, while convection and microphysics moisten by 0.3 and 0.7 ppmv, respectively (Figure 9 and Table 1). These results are in qualitative agreement with the case study results of *Ueyama et al*. [2014] and the results of *Schoeberl et al*. [2014] who used a different reanalysis, a model-derived convection product and a simpler, zero-dimensional cloud parcel model.

The tropical mean cloud occurrence frequencies at and above the cold point ~17 km agree well with those based on CALIPSO observations, where waves and convection enhance cloud occurrence at the cold point by ~4% and ~2%, respectively (Figure 6). The model-CALIPSO discrepancy may actually be larger given that a substantial fraction of the optically thin subvisible cirrus clouds near the tropical tropopause are below the detection limit of space-based lidars such as CALIPSO [*Davis et al*., 2010]. Incomplete diurnal and regional sampling issues of the CALIPSO data also contribute to the uncertainties. Nonetheless, the spatial distribution of the cloud occurrence frequency averaged over the 16–18 km layer is remarkably well correlated with CALIPSO measurements ($r = 0.82$), albeit with small displacements of the model clouds and overestimation over the eastern Pacific and Indian Ocean (Figure 7). In general, clouds in the middle to upper TTL are most frequently observed over the western and central Pacific, Northern Australia, South America, and Southern

Africa. Below the cold point, the model overestimates the cloud abundance by 5%, possibly due to excessive convective influence (enhancement of up to 17% in the lower TTL; Figure 6b). Both waves and convection raise the altitude of the final dehydration closer to the cold point tropopause (Figure 8b), but the latitudinal and longitudinal distributions of the final dehydration locations are robust and insensitive to various model parameters.

Here we evaluate the accuracy of the ERA-Interim temperature field, as well as the limitations of our trajectory model approach, to reconcile the discrepancies between the simulated result and observations, namely, the 0.7 ppmv dry bias at the 100 hPa level and the 5% overestimation of middle to lower TTL cloud abundance.

1. Since temperature is the single most important factor controlling the TTL dehydration process, temperatures from ERA-Interim reanalysis (with *Kim and Alexander* [2013] wave scheme) and tropical radiosonde stations in the World Meteorological Organization global network were compared. Twice daily, radiosonde soundings were screened for quality by selecting soundings with (i) uppermost reported level $\leq$70 hPa, (ii) cold point temperature *not* on mandatory pressure levels, and (iii) data reported at $\geq$5 levels between 70 and 150 hPa. Only the stations with $\geq$60 good soundings during December 2006 and February 2007 were used for the comparison, though results were not sensitive to the radiosonde selection criteria. Averaged over all selected radiosonde station locations during boreal winter 2006–2007, the cold point temperature of ERA-Interim with enhanced waves is approximately 0.3 K *warmer* than that of radiosondes (not shown), indicating that the model dry bias at 100 hPa is not likely due to the ERA-Interim cold point temperature bias. However, the TTL (70–150 hPa) mean temperatures of ERA-Interim are colder than those of radiosondes by 0.2 K, which may partly explain the overestimation of cloud occurrence frequencies below the cold point.
2. The role of temporal variability in the radiative heating rates was addressed by comparing the simulations using seasonal mean and 6-hourly ERA-Interim heating rates (section 3.4 and Table 1). The overall impact of the heating rate variability was to dehydrate the 100 hPa level by 0.4 ppmv and to decrease the cloud occurrence by 4%, suggesting that temporal variations in *Yang et al*. [2010] heating rates, if available, would likely exacerbate our model's dry bias but improve its cloud simulation. The sensitivity of our results to small differences in the heating rate field indicates the importance of radiative heating rates in determining TTL humidity and clouds. Small-scale convection driven by TTL cirrus radiative heating, which is not considered in this study, may also play a significant role, as shown in *Dinh and Fueglistaler* [2014].
3. The convection scheme consists of various parameters whose values were chosen such that the convective cloud top distribution in the model (Figure 3) agrees with estimates from CALIPSO and CloudSat observations. However, convective cloud top potential temperature is not a measured quantity, and the uncertainties of the observed estimates pose a challenge in constraining the parameter values. While our results are not particularly sensitive to a realistic range of values of the environmental to plume air mixing ratio of the convection scheme (not shown), parameters that affect the height distribution of convective detrainment require further investigation. We have shown that convective ice injection moistens the 100 hPa level by 0.5 to 0.6 ppmv (Table 1), possibly accounting for most of the dry bias of the base simulation. Additional improvements to the modeling of convection may potentially have a significant impact on the simulated water and clouds in the lower TTL where convective influence dominates.
4. The relative importance of homogeneous and heterogeneous nucleation in the TTL is not well known. While the details of the nucleation scheme do not appear to affect the 100 hPa level humidity, their impact on the cloud occurrence frequencies is significant. Heterogeneous ice nucleation increases cloud occurrence by 2–3%, while an increase in the ice saturation ratio threshold from ~1.3 to ~1.6 decreases cloud occurrence by 4% (Table 1). We have assumed homogeneous ice nucleation only in our base simulation, but both nucleation processes may be required for simulating realistic TTL cirrus clouds that are in better agreement with CALIPSO observations.
5. Our simulations assume no vertical wind shear of the horizontal wind along the 60 day trajectory paths, which is a clear limitation of the one-dimensional model. For example, the laminar structure of observed TTL cirrus clouds is likely due to vertically stacked thin layers of air masses coming from different directions. The lack of shear in our model will limit our ability to simulate observed clouds at specific locations at specific times, which may explain the zonal and meridional shifts in the model cloud locations compared to CALIPSO observations (Figure 7). However, given that the cloud lifetimes are typically on the order of 1–2 days [*Jensen et al*., 2011], the vertical profiles of H_2O and clouds during the dehydration and rehydration events should be reasonably insensitive to shear effects.

6. In-mixing of air from the extratropics are simulated in our model to the extent that some parcels cross the northern and southern tropical boundaries and hence are exposed to extratropical temperatures. However, our one-dimensional model ignores small-scale horizontal mixing between neighboring parcels along their trajectories. Subgrid-scale mixing in a three-dimensional model is estimated to increase the 100 hPa H_2O mixing ratio by approximately 0.5 ppmv [*Riese et al*., 2012; *Ploeger et al*., 2013], which may partly account for the dry bias in our model.
7. Vertical diffusivity is an important parameter in numerical models of tracer transport. We have neglected explicit treatment of the vertical diffusion of H_2O in the base simulation for simplicity; observational estimates of vertical diffusivity in the lower stratosphere range widely from 0.01 to 1.0 $m^2 s^{-1}$ [*Fukao et al*., 1994; *Mote et al*., 1998; *Alisse et al*., 2000; *Legras et al*., 2003; *Park et al*., 2010]. Since vertical diffusion is present in the real atmosphere, particularly in regions of wave-driven thermal instability and active convection, we examined the sensitivity of TTL humidity to moderate vertical diffusion based on a random set of 100 trajectories (out of a total 3780 trajectories in the base simulation). Preliminary results indicate that an increase in vertical diffusivity coefficient by 2 orders of magnitude (from 0.001 to 0.1 $m^2 s^{-1}$) moistens near the cold point tropopause by approximately 0.5 ppmv (not shown). The lack of vertical diffusion in our model may in part explain the dry bias at 100 hPa, but a more reliable estimate of its impact on the vertical transport of H_2O in the TTL requires better constraint on the vertical diffusivity coefficient in the TTL.

These results have important implications for the long-term variability and trend in stratospheric H_2O and future climate predictions. There has been considerable interest in quantifying and understanding the causes of global stratospheric H_2O trend [*Rosenlof et al*., 2001; *Hegglin et al*., 2014]. While seasonal to interannual variations in stratospheric H_2O have been linked to modulations in tropical tropopause temperature and the associated freeze-drying process [e.g., *Mote et al*., 1996; *Randel et al*., 2004; *Dessler et al*., 2013, 2014; *Wang et al*., 2015], their relationship on a longer time scale and in future climate is less clear. Yet current global chemistry climate models unanimously predict an increase in global stratospheric H_2O driven primarily by an increase in cold point tropopause temperature [*Gettelman et al*., 2010] implying that secondary processes involving cloud microphysics, convection, and wave activity are largely assumed to remain constant in time. This assumption is problematic because, as shown in this study, variations in atmospheric constituents that influence microphysical processes and factors that control the convective cloud top height and/or wave activity could cause stratospheric H_2O to vary independently of tropical tropopause temperature. For example, increasing sea surface temperatures in a warmer climate may generate stronger and deeper convection that transports more H_2O into the TTL. Deep convection in turn could enhance wave activity in the vicinity of the cold point and increase dehydration. *Kim and Alexander* [2015] have indeed shown that wave activity in the TTL has varied over the past few decades. These processes, through their influence on TTL cirrus abundance, can also directly alter the TTL thermal budget and the top of the atmosphere radiative forcing, amplifying the climate response through positive cloud feedback processes. Increasing aerosol emissions (e.g., from biomass burning) may alter ice crystal size and number distributions that affect TTL cirrus characteristics and its dehydration efficiency. The results of this study suggest the potentially important role of these TTL processes in stratospheric H_2O trend and variability and argue for improved representation of these processes in global models.

Acknowledgments

We would like to thank Mark Schoeberl, Tao Wang, and an anonymous reviewer for thoughtful and helpful comments. We also thank the Aura Science Team for the MLS data (http://mls.jpl.nasa.gov/), the CALIPSO science team for the cloud profile data (https://eosweb.larc.nasa.gov/project/calipso/calipso_table), and ECMWF for the ERA-Interim data (http://apps.ecmwf.int/datasets/data/interim_full_daily/). This work was funded by the NASA Airborne Tropical Tropopause Experiment, NASA Upper-Atmosphere Research Program, and the NASA Postdoctoral Program.

References

Alisse, J.-R., P. H. Haynes, J. Vanneste, and C. Sidi (2000), Quantification of stratospheric mixing from turbulent microstructure measurements, *Geophys. Res. Lett.*, *27*(17), 2621–2624, doi:10.1029/2000GL011386.

Bergman, J. W., E. J. Jensen, L. Pfister, and Q. Yang (2012), Seasonal differences of vertical-transport efficiency in the tropical tropopause layer: On the interplay between tropical deep convection, large-scale vertical ascent, and horizontal circulations, *J. Geophys. Res.*, *117*, D05302, doi:10.1029/2011JD016992.

Bonazzola, M., and P. H. Haynes (2004), A trajectory-based study of the tropical tropopause region, *J. Geophys. Res.*, *109*, D20112, doi:10.1029/2003JD004356.

Brewer, A. W. (1949), Evidence for a world circulation provided by the measurements of helium and water vapour distribution in the stratosphere, *Q. J. R. Meteorol. Soc.*, *75*, 351–363, doi:10.1002/qj.49707532603.

Cziczo, D. J., K. D. Froyd, C. Hoose, E. J. Jensen, M. Diao, M. A. Zondlo, J. B. Smith, C. H. Twohy, and D. M. Murphy (2013), Clarifying the dominant sources and mechanisms of cirrus cloud formation, *Science*, *340*(6138), 1320–1324, doi:10.1126/science.1234145.

Davis, S., et al. (2010), In situ and lidar observations of tropopause subvisible cirrus clouds during TC4, *J. Geophys. Res.*, *115*, D00J17, doi:10.1029/2009JD013093.

Dee, D. P., et al. (2011), The ERA-interim reanalysis: Configuration and performance of data assimilation system, *Q. J. R. Meteorol. Soc.*, *137*, 553–597, doi:10.1002/qj.828.

Dessler, A. E., M. R. Schoeberl, T. Wang, S. M. Davis, and K. H. Rosenlof (2013), Stratospheric water vapor feedback, *Proc. Natl. Acad. Sci. U.S.A.*, *110*, 18,087–18,091, doi:10.1073/pnas.1310344110.

Dessler, A. E., M. R. Schoeberl, T. Wang, S. M. Davis, K. H. Rosenlof, and J.-P. Vernier (2014), Variations of stratospheric water vapor over the past three decades, *J. Geophys. Res. Atmos.*, *119*, 12,588–12,598, doi:10.1002/2014JD021712.

Dinh, T., and S. Fueglistaler (2014), Microphysical, radiative, and dynamical impacts of thin cirrus clouds on humidity in the tropical tropopause layer and lower stratosphere, *Geophys. Res. Lett.*, *41*, 6949–6955, doi:10.1002/2014GL061289.

Froyd, K. D., D. Murphy, T. J. Sanford, D. S. Thomson, J. Wilson, L. Pfister, and L. R. Lait (2009), Aerosol composition of the tropical upper troposphere, *Atmos. Chem. Phys.*, *9*, 4363–4385, doi:10.5194/acp-9-4363-2009.

Fueglistaler, S., and M. B. Baker (2006), A modeling study of the impact of cirrus clouds on the moisture budget of the upper troposphere, *Atmos. Chem. Phys.*, *6*, 1425–1434, doi:10.5194/acp-6-1425-2006.

Fueglistaler, S., A. E. Dessler, T. J. Dunkerton, I. Folkins, Q. Fu, and P. W. Mote (2009), Tropical tropopause layer, *Rev. Geophys.*, *47*, RG1004, doi:10.1029/2008RG00267.

Fukao, S., M. D. Yamanaka, N. Ao, W. K. Hocking, T. Sato, M. Yamamoto, T. Nakamura, T. Tsuda, and S. Kato (1994), Seasonal variability of vertical eddy diffusivity in the middle atmosphere: 1. Three-year observations by the middle and upper atmosphere radar, *J. Geophys. Res.*, *99*(D9), 18,973–18,987, doi:10.1029/94JD00911.

Gettelman, A., W. J. Randel, F. Wu, and S. T. Massie (2002a), Transport of water vapor in the tropical tropopause layer, *Geophys. Res. Lett.*, *29*(1), 1009, doi:10.1029/2001GL013818.

Gettelman, A., M. L. Salby, and F. Sassi (2002b), Distribution and influence of convection in the tropical tropopause region, *J. Geophys. Res.*, *107*(D10), 4080, doi:10.1029/2001JD001048.

Gettelman, A., et al. (2009), The tropical tropopause layer 1960–2100, *Atmos. Chem. Phys.*, *9*, 1621–1637, doi:10.5194/acp-9-1621-2009.

Gettelman, A., et al. (2010), Multimodel assessment of the upper troposphere and lower stratosphere: Tropics and global trends, *J. Geophys. Res.*, *115*, D00M08, doi:10.1029/2009JD013638.

Hegglin, M. I., et al. (2014), Vertical structure of stratospheric water vapour trends derived from merged satellite data, *Nat. Geosci.*, *7*, 768–776, doi:10.1038/ngeo2236.

Holton, J. R., and A. Gettelman (2001), Horizontal transport and the dehydration of the stratosphere, *Geophys. Res. Lett.*, *298*(14), 2799–2802, doi:10.1029/2001GL013148.

Holton, J. R., P. H. Haynes, M. E. McIntyre, A. R. Douglass, R. B. Rood, and L. Pfister (1995), Stratosphere-troposphere exchange, *Rev. Geophys.*, *33*(4), 403–439, doi:10.1029/95RG02097.

Jensen, E. J., and A. S. Ackerman (2006), Homogeneous aerosol freezing in the tops of high-altitude tropical cumulonimbus clouds, *Geophys. Res. Lett.*, *33*, L08802, doi:10.1029/2005GL024928.

Jensen, E. J., and L. Pfister (2004), Transport and freeze-drying in the tropical tropopause layer, *J. Geophys. Res.*, *109*, D02207, doi:10.1029/2003JD004022.

Jensen, E. J., et al. (2009), On the importance of small ice crystals in tropical anvil cirrus, *Atmos. Chem. Phys.*, *9*, 5519–5537.

Jensen, E. J., L. Pfister, and O. B. Toon (2011), Impact of radiative heating, wind shear, temperature variability, and microphysical processes on the structure and evolution of thin cirrus in the tropical tropopause layer, *J. Geophys. Res.*, *116*, D12209, doi:10.1029/2010JD015417.

Jensen, E. J., D. Glenn, R. Paul Lawson, L. Sara, T. Paul Bui, D. Hlavka, M. McGill, L. Pfister, O. B. Toon, and R. Gao (2013), Ice nucleation and dehydration in the Tropical Tropopause Layer, *Proc. Natl. Acad. Sci. U.S.A.*, *110*(6), 2041–2046, doi:10.1073/pnas.1217104110.

Kim, J.-E., and M. J. Alexander (2013), A new wave scheme for trajectory simulations of stratospheric water vapor, *Geophys. Res. Lett.*, *40*, 5286–5290, doi:10.1002/grl.50963.

Kim, J.-E., and M. J. Alexander (2015), Direct impacts of waves on tropical cold point tropopause temperature, *Geophys. Res. Lett.*, *42*, 1584–1592, doi:10.1002/2014.GL062737.

Knollenberg, R. G., K. Kelly, and J. C. Wilson (1993), Measurements of high number densities of ice crystals in the tops of tropical cumulonimbus, *J. Geophys. Res.*, *98*(D5), 8639–8664, doi:10.1029/92JD02525.

Koop, T., B. Luo, A. Tsias, and T. Peter (2000), Water activity as the determinant for homogeneous ice nucleation in aqueous solutions, *Nature*, *406*, 611–614, doi:10.1038/35020537.

Legras, B., B. Joseph, and F. Lefèvre (2003), Vertical diffusivity in the lower stratosphere from Lagrangian back-trajectory reconstructions of ozone profiles, *J. Geophys. Res.*, *108*(D18), 4562, doi:10.1029/2002JD003045.

Liu, C., E. J. Zipser, and S. W. Nesbitt (2007), Global distribution of tropical deep convection: Different perspectives from TRMM infrared and radar data, *J. Clim.*, *20*, 489–503, doi:10.1175/JCLI4023.1.

Liu, Y. S., S. Fueglistaler, and P. H. Haynes (2010), Advection-condensation paradigm for stratospheric water vapor, *J. Geophys. Res.*, *115*, D24307, doi:10.1029/2010JD014352.

Luo, Z., G. Y. Liu, and G. L. Stephens (2008), CloudSat adding new insight into tropical penetrating convection, *Geophys. Res. Lett.*, *35*, L19819, doi:10.1029/2008GL035330.

Mote, P. W., K. H. Rosenlof, M. E. McIntyre, E. S. Carr, J. C. Gille, J. R. Holton, J. S. Kinnersley, H. C. Pumphrey, J. M. Russell III, and J. W. Waters (1996), An atmospheric tape-recorder: The imprint of tropical tropopause temperatures on stratospheric water vapor, *J. Geophys. Res.*, *101*(D2), 3989–4006, doi:10.1029/95JD03422.

Mote, P. W., T. J. Dunkerton, M. E. McIntyre, E. A. Ray, P. H. Haynes, and J. M. Russell III (1998), Vertical velocity, vertical diffusion, and dilution by midlatitude air in the tropical lower stratosphere, *J. Geophys. Res.*, *103*(D8), 8651–8666, doi:10.1029/98JD00203.

Park, S., et al. (2010), Vertical transport rates and concentrations of OH and Cl radicals in the Tropical Tropopause Layer from observations of CO_2 and halocarbons: Implications for distributions of long- and short-lived chemical species, *Atmos. Chem. Phys.*, *10*, 6669–6683, doi:10.5194/acp-10-6669-2010.

Pfister, L., et al. (2001), Aircraft observations of thin cirrus clouds near the tropical tropopause, *J. Geophys. Res.*, *106*(D9), 9765–9786, doi:10.1029/2000JD900648.

Ploeger, F., G. Günther, P. Konopka, S. Fueglistaler, R. Müller, C. Hoppe, A. Kunz, R. Spang, J.-U. Grooß, and M. Riese (2013), Horizontal water vapor transport in the lower stratosphere from subtropics to high latitudes during boreal summer, *J. Geophys. Res. Atmos.*, *118*, 8111–8128, doi:10.1002/jgrd.50636.

Poli, P., S. B. Healy, and D. P. Dee (2010), Assimilation of Global Positioning System radio occultation data in the ECMWF ERA-Interim reanalysis, *Q. J. R. Meteorol. Soc.*, *136*, 1972–1990, doi:10.1002/qj.722.

Randel, W. J., and E. J. Jensen (2013), Physical processes in the tropical tropopause layer and their roles in a changing climate, *Nat. Geosci.*, *6*(3), 169–176, doi:10.1038/ngeo1733.

Randel, W. J., F. Wu, S. J. Oltmans, K. Rosenlof, and G. E. Nedoluha (2004), Interannual changes of stratospheric water vapor and correlations with tropical tropopause temperatures, *J. Atmos. Sci.*, *61*, 2133–2148, doi:10.1175/1520-0469(2004)061<2133:ICOSWV>2.0.CO;2.

Read, W. G., et al. (2007), Aura Microwave Limb Sounder upper tropospheric and lower stratospheric H2O and relative humidity with respect to ice validation, *J. Geophys. Res.*, *112*, D24S35, doi:10.1029/2007JD008752.

Reinecker, M. M., et al. (2011), MERRA: NASA's Modern-Era Retrospective Analysis for Research and Applications, *J. Clim.*, *24*, 3624–3648, doi:10.1175/JCLI-D-11-00015.1.

Riese, M., F. Ploeger, A. Rap, B. Vogel, P. Konopka, M. Dameris, and P. Forster (2012), Impact of uncertainties in atmospheric mixing on simulated UTLS composition and related radiative effects, *J. Geophys. Res.*, *117*, D16305, doi:10.1029/2012JD017751.

Rosenlof, K., et al. (2001), Stratospheric water vapor increases over the past half-century, *Geophys. Res. Lett.*, *28*(7), 1195–1198, doi:10.1029/2000GL012502.

Schiller, C., J.-U. Grooβ, P. Konopka, F. Plöger, F. H. Silva dos Santos, and N. Spelten (2009), Hydration and dehydration at the tropical tropopause, *Atmos. Chem. Phys.*, *9*, 9647–9660, doi:10.5194/acp-9-9647-2009.

Schoeberl, M. R., and A. E. Dessler (2011), Dehydration of the stratosphere, *Atmos. Chem. Phys.*, *11*, 8433–8446, doi:10.5194/acp-11-8433-2011.

Schoeberl, M. R., A. Dessler, and T. Wang (2013), Modeling upper tropospheric and lower stratospheric water vapor anomalies, *Atmos. Chem. Phys.*, *13*, 7783–7793, doi:10.5194/acp-13-7783-2013.

Schoeberl, M. R., A. Dessler, T. Wang, M. Avery, and E. J. Jensen (2014), Cloud formation, convection, and stratospheric dehydration, *Earth Space Sci.*, *1*, 1–17, doi:10.1002/2014EA000014.

Solomon, S., K. H. Rosenlof, R. W. Portmann, J. S. Daniel, S. M. Davis, T. J. Sanford, and G.-K. Plattner (2010), Contributions of stratospheric water vapor to decadal changes in the rate of global warming, *Science*, *327*, 1219–1223, doi:10.1126/science.1182488.

Ueyama, R., E. J. Jensen, L. Pfister, G. S. Diskin, T. P. Bui, and J. M. Dean-Day (2014), Dehydration in the tropical tropopause layer: A case study for model evaluation using aircraft observations, *J. Geophys. Res. Atmos.*, *119*, 5299–5316, doi:10.1002/2013JD021381.

Wang, T., W. J. Randel, A. E. Dessler, M. R. Schoeberl, and D. E. Kinnison (2014), Trajectory model simulations of ozone (O_3) and carbon monoxide (CO) in the lower stratosphere, *Atmos. Chem. Phys.*, *14*, 7135–7147, doi:10.5194/acp-14-7135-2014.

Wang, T., A. E. Dessler, M. R. Schoeberl, W. J. Randel, and J.-E. Kim (2015), The impact of temperature vertical structure on trajectory modeling of stratospheric water vapor, *Atmos. Chem. Phys.*, *15*, 3517–3526, doi:10.5194/acp-15-3517-2015.

Winker, D. M., M. A. Vaughan, A. Omar, Y. Hu, K. A. Powell, Z. Liu, W. H. Hunt, and S. A. Young (2009), Overview of the CALIPSO mission and CALIOP data processing algorithms, *J. Atmos. Oceanic Technol.*, *26*, 2310–2323, doi:10.1175/2009JTECHA1281.1.

Yang, Q., Q. Fu, and Y. Hu (2010), Radiative impacts of clouds in the tropical tropopause layer, *J. Geophys. Res.*, *115*, D00H12, doi:10.1029/2009JD012393.